Cell, Vol. 118, 389–401, August 6, 2004, Copyright ©2004 by Cell Press

Calmodulin and Munc13 Form a Ca^{2+} Sensor/Effector Complex that Controls Short-Term Synaptic Plasticity

Harald J. Junge,[1] Jeong-Seop Rhee,[3] Olaf Jahn,[2] Frederique Varoqueaux,[1] Joachim Spiess,[2] M. Neal Waxham,[4] Christian Rosenmund,[3] and Nils Brose[1,*]

[1]Department of Molecular Neurobiology
[2]Department of Molecular Neuroendocrinology
Max-Planck-Institute for Experimental Medicine
Hermann-Rein-Straße 3
D-37075 Göttingen
[3]Department of Membrane Biophysics
Max-Planck-Institute for Biophysical Chemistry
Am Faßberg 11
D-37077 Göttingen
Germany
[4]Department of Neurobiology and Anatomy
University of Texas Medical School at Houston
Houston, Texas 77030

Summary

The efficacy of synaptic transmission between neurons can be altered transiently during neuronal network activity. This phenomenon of short-term plasticity is a key determinant of network properties; is involved in many physiological processes such as motor control, sound localization, or sensory adaptation; and is critically dependent on cytosolic [Ca^{2+}]. However, the underlying molecular mechanisms and the identity of the Ca^{2+} sensor/effector complexes involved are unclear. We now identify a conserved calmodulin binding site in UNC-13/Munc13s, which are essential regulators of synaptic vesicle priming and synaptic efficacy. Ca^{2+} sensor/effector complexes consisting of calmodulin and Munc13s regulate synaptic vesicle priming and synaptic efficacy in response to a residual [Ca^{2+}] signal and thus shape short-term plasticity characteristics during periods of sustained synaptic activity.

Introduction

Neurons transfer information at chemical synapses. Interestingly, synaptic activity does not only transmit information but also regulates synaptic strength. Such activity-dependent modification of synaptic performance, or synaptic plasticity, is essential for information processing, learning, and memory.

Short-term synaptic plasticity (STP) occurs during and after repetitive synaptic activity on a timescale of milliseconds to minutes. It is a key determinant of network processes and is involved in brain functions as diverse as motor control (Nadim and Manor, 2000), sensory adaptation (Chung et al., 2002), sound localization (Cook et al., 2003), and cortical gain control (Abbott et al., 1997). STP can be expressed either as short-term enhancement (STE) or short-term depression (STD), depending on the initial release probability (P_r) of the synapses involved. High P_r is usually associated with STD, while a low P_r favors STE (Zucker and Regehr, 2002).

Depletion of a readily releasable pool of fusion-competent synaptic vesicles (RRP) is a major cause for STD (Liley and North, 1953). The generation of this RRP is absolutely dependent on the priming action of UNC-13/Munc13s (Varoqueaux et al., 2002; see below). The level of STD under steady-state conditions of RRP depletion and replenishment is controlled by a Ca^{2+}-dependent vesicle supply process, of which the molecular mechanism and significance for STP are poorly understood (Dittman and Regehr, 1998; Stevens and Wesseling, 1998; Wang and Kaczmarek, 1998). Calmodulin (CaM) may mediate this Ca^{2+}-dependent process by acting on a subpool of the RRP with high P_r (Sakaba and Neher, 2001).

A second well-known form of STP is STE (Eccles et al., 1941; Feng, 1941). Three major forms of STE, facilitation, augmentation, and potentiation, can be distinguished based on their lifetime (Zucker and Regehr, 2002). During sustained activity, the efficacy of release is increased in STE, but it is unclear whether this is due to increased vesicular P_r or RRP size or both. STE is critically dependent on increased concentrations of residual Ca^{2+} ($[Ca^{2+}]_{res}$), which accumulates during action potential activity due to incomplete elimination. According to the original residual Ca^{2+} hypothesis (Katz and Miledi, 1968), $[Ca^{2+}]_{res}$ was thought to act on the secretory Ca^{2+} sensor. However, given the differences in Ca^{2+} requirements of fast neurotransmitter release and STE, additional, high-affinity Ca^{2+} sensors likely contribute to STE (Zucker and Regehr, 2002). The identification of such high-affinity Ca^{2+} sensors whose characteristics are compatible with the Ca^{2+} dynamics in presynaptic terminals and of molecules that transduce the residual Ca^{2+} signal to the secretory machinery during STE is essential for a mechanistic understanding of STE.

The Munc13 proteins (Munc13-1, the splice isoforms bMunc13-2 and ubMunc13-2, and Munc13-3) are candidate mediators of STP (Rosenmund et al., 2002). Genetic studies in mouse, fly, and nematode have established an essential role for this presynaptic protein family in synaptic vesicle priming and RRP generation (Aravamudan et al., 1999; Augustin et al., 1999; Richmond et al., 1999). Munc13s regulate the SNARE protein Syntaxin (Betz et al., 1997) and promote SNARE complex formation and fusion competence of synaptic vesicles (Brose et al., 2000; Richmond et al., 2001).

By determining synaptic vesicle priming, Munc13s modify synaptic strength. The domain structure of Munc13s with several binding sites for second messengers and regulatory proteins indicates that this function is tightly regulated. Indeed, Munc13s are targets of the diacylglycerol (DAG) second messenger pathway. The C_1 domain function of Munc13-1 is essential for DAG and phorbol ester (PE) binding and PE potentiation of synaptic amplitudes in hippocampal neurons (Rhee et al., 2002). Moreover, rescue experiments in Munc13-1/2 double knockout (DKO) neurons showed that STE is

*Correspondence: brose@em.mpg.de

prevalent in neurons that express only ubMunc13-2, while moderate STD is prominent in neurons expressing only Munc13-1 (Rosenmund et al., 2002). Thus, Munc13 isoforms can differentially control STP, but the relation of this phenomenon to the long-established role of $[Ca^{2+}]_{res}$ in STP is unknown.

We report here that Munc13-1 and ubMunc13-2 bind CaM in a Ca^{2+}-dependent manner via an evolutionarily conserved CaM recognition motif. Using synaptic depression, frequency facilitation, and augmentation protocols in autaptic hippocampal neurons as a model of STP, we show that CaM binding to Munc13 proteins causes increased priming activity and RRP sizes. We conclude that activation of the CaM/Munc13 complex by $[Ca^{2+}]_{res}$ represents a molecular correlate for the phenomenon of Ca^{2+}-dependent vesicle pool refilling. This mechanism controls STP characteristics and is likely to be evolutionarily conserved.

Results

Munc13-1 and ubMunc13-2 Bind CaM via a Conserved Binding Site

To identify proteins that regulate the function of Munc13s in presynaptic neurotransmitter release, we searched for interactors of Munc13-1 and ubMunc13-2 using the yeast two-hybrid (YTH) system. Using a rat Munc13-1 bait (aa 441–1181) in pLexN, we identified CaM as a Munc13-1 binding protein. From a total of 50 million yeast clones cotransformed with the bait construct and a rat E16 brain library in pVP16-3, all 77 isolated and sequenced positive clones encoded full-length cDNAs or fragments of the three CaM genes *calm1*, *calm2*, and *calm3* (Figure 1C). Sequences of seven of the prey clones encoded N-terminally truncated CaM. In all these cases, the C-terminal CaM lobe with EF hands three and four remained intact, indicating that this lobe is sufficient to bind Munc13-1.

Munc13-1 and the ubiquitously expressed splice variant of Munc13-2, ubMunc13-2, as well as the *C. elegans* LR UNC-13 splice variant, contain homologous N termini whose first 150 residues bind the active zone protein RIM1 (Betz et al., 2001; Koushika et al., 2001). We therefore performed a second screen with residues 273–408 of rat ubMunc13-2 in the pLexN bait vector and a rat P8 brain library in pVP16-3. From 8 million cotransformants, 39 positive clones were isolated and analyzed. Most of these clones (33) encoded CaM or N-terminally truncated CaM fragments (Figure 1D). Again, all truncations contained at least the C-terminal CaM lobe with EF hands three and four. This finding may be due to the fact that the C-terminal lobe binds Ca^{2+} with 5-fold higher affinity than the N-terminal lobe (Chin and Means, 2000).

Neither the pVP16-3-CaM prey constructs nor the bait constructs had autoactivating properties, indicating that the CaM interaction with Munc13s is highly specific. The results of both screens are essentially identical, indicating that a CaM binding site is present in the region N-terminal of the C_1 domain where both bait constructs overlap (Figure 1A).

To verify the CaM/Munc13 interaction with an independent method and to examine the Ca^{2+} dependence

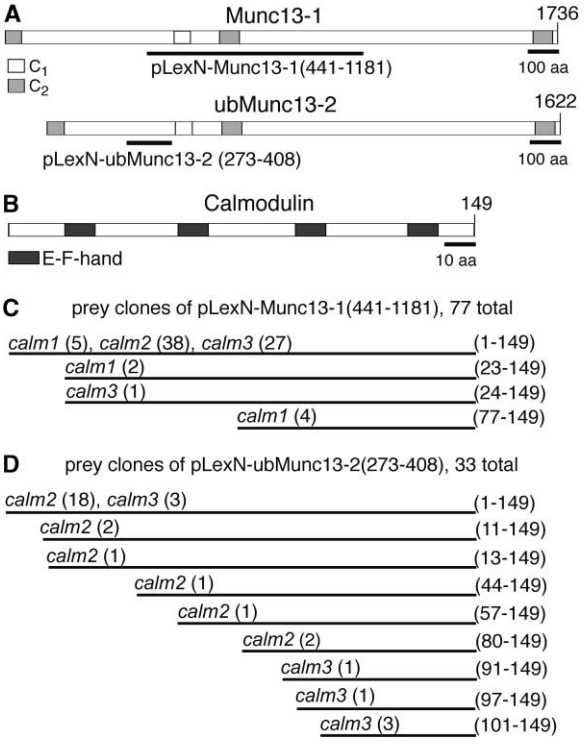

Figure 1. YTH Screens Identify CaM as an Interactor of Munc13-1 and ubMunc13-2

(A) Domain structures of Munc13-1 and ubMunc13-2 and representation of Munc13-1 and ubMunc13-2 bait constructs (black bars) used in YTH screens.

(B) Domain structure of CaM.

(C and D) Representation of CaM prey clones identified in screens with pLexN-Munc13-1(441–1181) (C) and pLexN-ubMunc13-2(273–408) (D). The prey cDNA clones originate from three CaM genes (*calm1, calm2, calm3*). Black bars indicate areas represented by prey clones relative to the domain structure shown in (B). Numbers in brackets behind the black bars indicate the CaM sequence covered by the indicated clones. Individual numbers in brackets behind the CaM gene name denote the number of clones of a particular type isolated in the screen.

of this interaction, we performed cosedimentation experiments. Fusion proteins of Munc13 fragments with GST were expressed in bacteria, immobilized on glutathione agarose beads, and tested for CaM binding using rat brain synaptosome extracts in the presence of 1 mM EGTA or 2 mM Ca^{2+}. GST-Munc13-1(1–847), GST-Munc13-1(309–567), and GST-Munc13-1(445–567) bound CaM in the presence of Ca^{2+}, while GST alone, GST-Munc13-1(1–455), or GST-Munc13-1(514–1735) did not (Figure 2B). CaM binding to GST-Munc13-1(445–567) was only partially Ca^{2+} dependent, while binding to the other Munc13-1 constructs was strictly Ca^{2+} dependent. Together, these results indicate that CaM binding to Munc13-1 is restricted to a small sequence stretch (residues 445–567) N-terminal of the C_1 domain. The homologous sequence in ubMunc13-2 (residues 372–494) also bound CaM in a specific and Ca^{2+}-dependent manner (Figure 5A).

Most CaM targets carry one of two types of CaM recognition motifs, predominantly Ca^{2+}-independent IQ motifs (with prominent I and Q residues), or predomi-

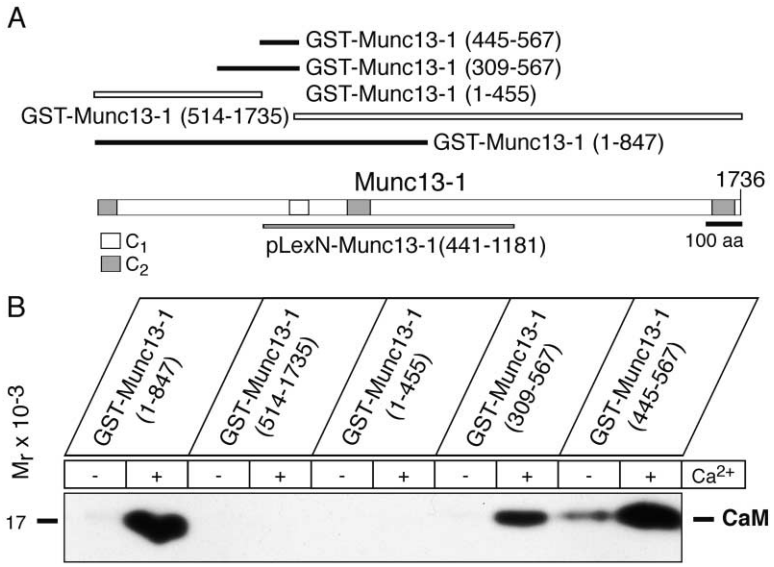

Figure 2. The CaM Binding Site in Munc13-1 and ubMunc13-2 Maps to a Short Sequence Stretch N-Terminal to the C_1 Domain

(A) Domain structure of Munc13-1 (bottom) and representation of GST-Munc13-1 fusion proteins (black and white bars) used for the analysis of CaM binding in cosedimentation experiments. Black bars indicate CaM binding, white bars lack of binding. The gray bar indicates the YTH bait construct used in the present study (see Figure 1A).

(B) CaM binding to GST-Munc13-1 fusion proteins in cosedimentation assays. Identical amounts of the indicated GST fusion proteins containing Munc13-1 sequences were immobilized and used in cosedimentation assays with rat brain synaptosome extract in the presence or absence of Ca^{2+}. Proteins that bound to the immobilized fusion proteins were analyzed by immunoblotting. Only fusion proteins containing a region N-terminal to the C_1 domain bound CaM (see [A]).

nantly Ca^{2+}-dependent 1-5-10 or 1-8-14 motifs and their derivatives (Rhoads and Friedberg, 1997). The latter are defined by amphipathic helices with a net positive charge, in which hydrophobic residues occur preferentially at positions 1-5-10 or 1-8-14. We thus searched for CaM binding motifs in Munc13s using secondary structure prediction tools. In Munc13-1 and ubMunc13-2, the presence of an amphipathic helix with a net positive charge was predicted in the region N-terminal of the C_1 domain (Munc13-1, residues 460–477; ubMunc13-2, residues 383–400). In these helices, clusters of hydrophobic residues are separated from clusters of polar and charged, mostly basic residues (Figure 3A and 3B).

An alignment of the predicted amphipathic helices within the CaM binding regions of rat Munc13-1 and ubMunc13-2 with available sequences of UNC-13/Munc-13 proteins from human, *C. elegans*, and *D. melanogaster* reveals significant homology. Interestingly, hydrophobic, basic, and helix-promoting residues are conserved across all isoforms and species (Figure 3C). These conserved residues represent elements of a predominantly Ca^{2+}-dependent CaM recognition motif. Within the amphipathic helix of several other CaM targets, the first hydrophobic anchor point in the N-terminal part of the motif is a Trp residue (Chin and Means, 2000). This characteristic Trp is also present and conserved in Munc13-1, ubMunc13-2, and their invertebrate homologs. Relative to this first hydrophobic anchor point,

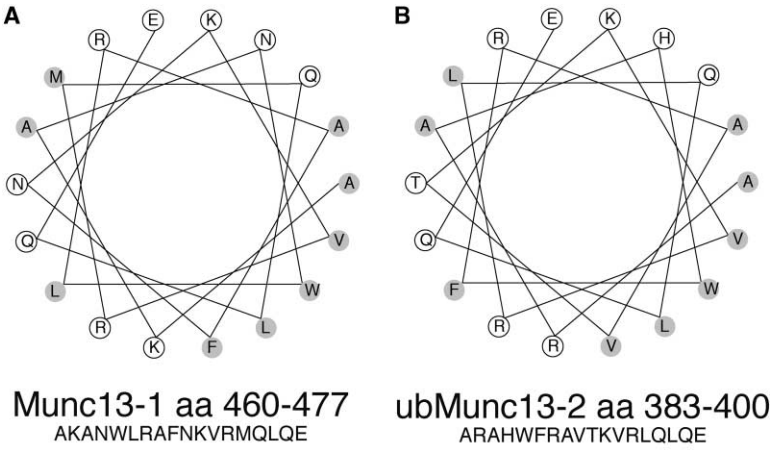

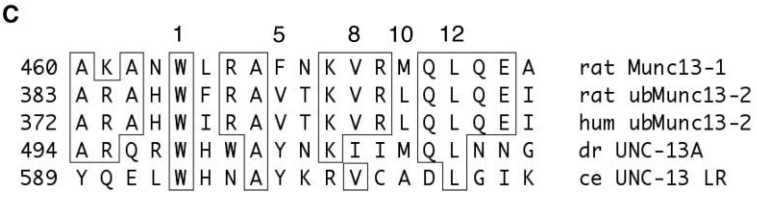

Figure 3. Helical Wheel Projections of the CaM Binding Site in Munc13-1 and ubMunc13-2 and Evolutionary Conservation

(A and B) Amphipathic helices predicted in the CaM binding regions of Munc13-1 and ubMunc13-2 expose clusters of hydrophobic (gray circles) and hydrophilic (open circles) amino acids. The overall structure of both helices is almost identical.

(C) Sequence alignment of putative CaM binding sites in Munc13/UNC-13 homologs. Net positive charge and spacing of hydrophobic anchor points for CaM are conserved across all species (see text).

other conserved hydrophobic residues follow at positions 4, 8, 10, and 12. Interestingly, parallel and independent studies, which aimed to identify CaM binding proteins in *Drosophila*, have indicated that fly UNC-13 might also bind CaM (Xu et al., 1998).

The above data indicate that CaM binding to UNC-13/Munc13s is evolutionarily conserved. The vertebrate and invertebrate orthologs may employ distinct CaM recognition motif derivatives (1-5-10 in mammals and 1-8-14 in invertebrates), or UNC-13/Munc13s may contain a CaM recognition motif with hydrophobic anchor points at position 1-8-12. Due to its very flexible mode of target binding, CaM can recognize such derivatives of the regular motifs (Chin and Means, 2000).

To test the functionality of the predicted CaM binding sites in Munc13-1 and ubMunc13-2 (Figure 3), we synthesized peptides representing the amphipathic helices of both isoforms, Munc13-1(459–479) and ubMunc13-2(382–402), and tested their CaM binding characteristics. A photoactivatable benzophenone (Bp) label was coupled to the N-terminal NH_2 groups of the Munc13 peptides for photoaffinity labeling experiments (Jahn et al., 2002). In this position, the label was part of the hydrophobic patch of the helix.

Bp-Munc13-1 and Bp-ubMunc13-2 were efficiently crosslinked to purified CaM under reducing conditions and with CaM in slight excess (5 μM versus 4.5 μM). No crosslinking was observed in the absence of UV light or with purified GST instead of CaM (data not shown). Analysis of the crosslinking reaction by SDS-PAGE and Coomassie blue staining revealed two photoadducts with slightly higher apparent molecular mass than CaM (Figures 4A and 4B). Binding to CaM depended strongly on the presence of Ca^{2+} in the case of Bp-ubMunc13-2(382–402) (Figure 4B), while binding of Bp-Munc13-1(459–479) was partially Ca^{2+} independent (Figure 4A). When unlabeled peptides (1–37 μM) were used as specific competitors for binding, crosslinking of the photoprobes was successively inhibited with increasing inhibitor peptide concentration, indicating that labeled and unlabeled forms of the peptides bind the same binding site (Figures 4A and 4B).

Interactions of CaM with amphipathic target sequences usually have a 1:1 stoichiometry. Therefore, the observation that more than one additional band in SDS-PAGE gels occurs after crosslinking of CaM with Munc13 peptides is unexpected. To determine whether these bands correspond to isomeric 1:1 adducts, in which the peptide is bound to different residues of CaM, we analyzed the crosslinking reactions by liquid chromatography/electrospray mass spectrometry (LC-MS). In the total ion current chromatogram, the crosslinking products were represented by three peaks (brackets in Figures 4C and 4D), which was in agreement with the SDS-PAGE analysis. However, the deconvoluted mass spectra corresponding to the entire triple peak chromatography signal revealed the presence of only two main mass peaks in both reactions. In crosslinking experiments with CaM and Bp-Munc13-1(459–479), one peak (molecular mass of 16,786 Da) was identified as CaM (Mr_{calc}[CaM] = 16,790 Da) and the other as the photoadduct formed by CaM and Bp-Munc13-1(459–479) (mass increase of 2904 Da, matching Mr_{calc}[Bp-Munc13-1(459–479)] = 2897.4 Da) (Figure 4E). Thus, only unmodified CaM and a 1:1 adduct but no higher order adducts were detected (Figures 4E and 4F).

Together with the finding that only one CaM binding site is present on Munc13-1 (see Figures 2A and 5B), the LC-MS analysis demonstrates a 1:1 stoichiometry of the Munc13-1/CaM interaction. The double band/double peak observed for the photoadducts after electrophoretic or chromatographic separation of the crosslinking products likely represent two isomers of the CaM/Munc13-1(459–479) adduct. In the analysis of the Bp-Munc13-2(382–402)/CaM crosslink, we obtained a similar result (Figures 4D and 4F). CaM and the photoadduct formed by CaM and Bp-ubMunc13-2(382–402) were detected, which differed in their molecular weight by 2856 Da (matching Mr_{calc} [Bp-ubMunc13-2 (382–402)] = 2848.3 Da).

The UV-crosslinking results were confirmed with an alternative assay, in which we analyzed the fluorescence emission spectra of Munc13-1(459–479) and ubMunc13-2(382–402) before and after CaM binding (Figures 4G and 4H). Both peptides contain a Trp residue that was excited at 290 nm. Emission spectra of solutions containing 10 μM of either peptide in 0.25 M ammonium actetate (pH 8) were obtained between 300 and 430 nm, and the scans were repeated after addition of 10 μM CaM/EGTA and, finally, after adding an excess of Ca^{2+}. In the absence of additives, the emission of both peptides peaked at 355 nm. Addition of Ca^{2+}-free apoCaM resulted in a blueshift in the case of Munc13-1(459–479), indicating a change in the chemical environment of the reporter during binding. In the presence of Ca^{2+}, the blueshift was increased (peak emission at 324 nm with higher intensity). CaM, which does not contain Trp residues, did not emit significant fluorescence under these conditions. These findings are very similar to observations published on other peptides that represent Trp-based CaM recognition motifs (O'Neil and DeGrado, 1989). The changes in Trp fluorescence of ubMunc13-2(382–402) upon CaM binding were analogous but occurred only in the presence of Ca^{2+}/CaM and not apoCaM.

These experiments show that small 21-residue peptides representing the conserved CaM recognition motifs of Munc13-1 and ubMunc13-2 bind CaM specifically, directly, and with a 1:1 stoichiometry.

To identify residues in Munc13-1 and ubMunc13-2 that are essential for CaM binding, we introduced single point mutations into GST-Munc13-1(445–567) and GST-ubMunc13-2(372–494), which robustly bind CaM (Figure 5A), and tested for consequences on CaM binding in cosedimentation assays. We focused on the conserved Trp residue within the CaM recognition motifs of Munc13-1 and ubMunc13-2 because this residue has a prominent position in the binding site and changes its fluorescence emission upon CaM binding (Figures 4G and 4H). In both Munc13 isoforms, the Trp residue was mutated to Arg, which was predicted to be compatible with an α-helical structure. GST-Munc13-1(445–567)^{W464R} and GST-ubMunc13-2(372–494)^{W387R} were expressed, purified, and tested for CaM binding using synaptosome extracts. In both cases, Trp/Arg mutations abolished CaM binding completely (Figure 5A).

We assessed the effect of the Trp mutation in full-length Munc13s by expressing wild-type (wt) and Trp/

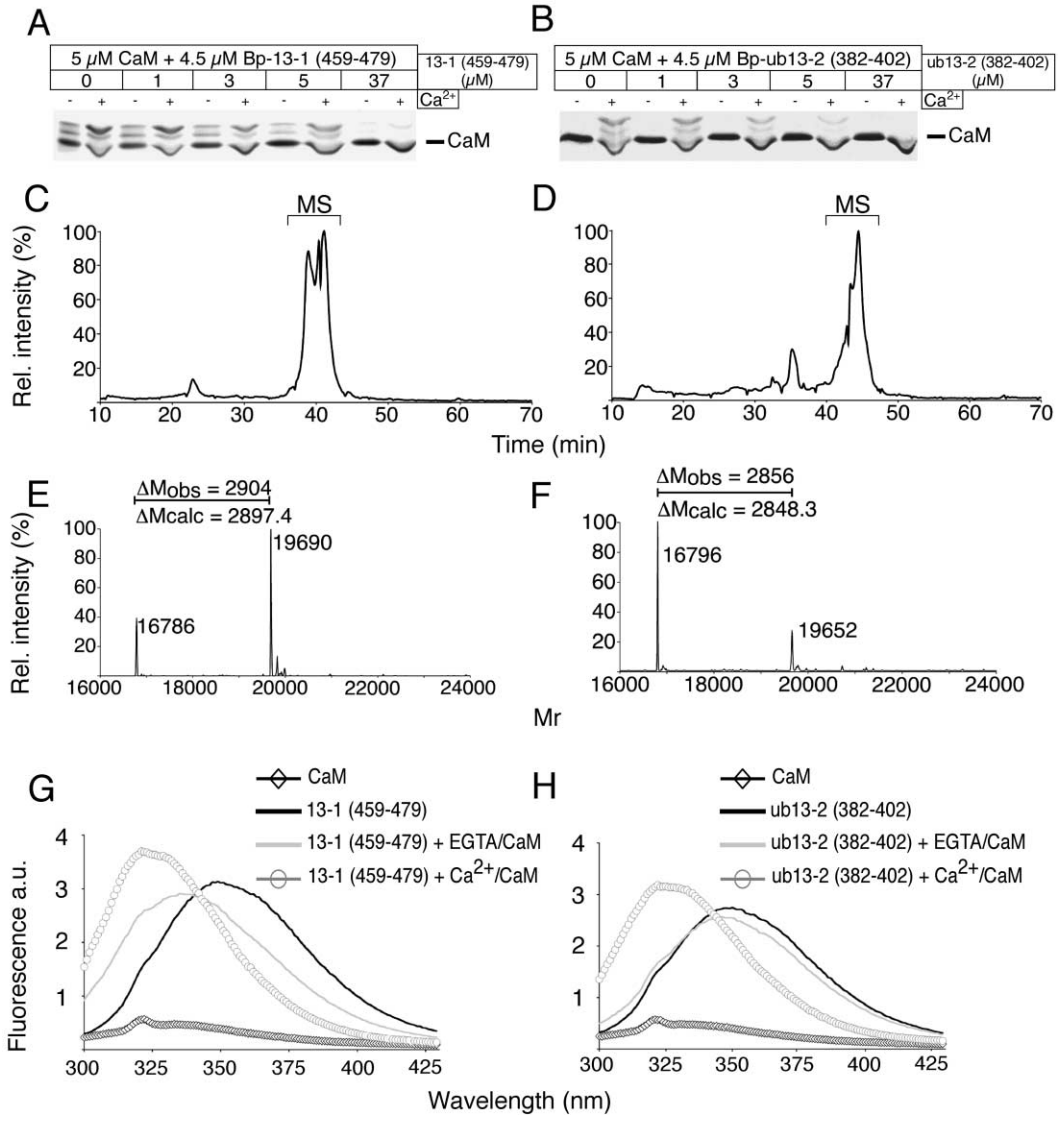

Figure 4. CaM Binding Sites of Munc13-1 and ubMunc13-2 Bind CaM with a 1:1 Stoichiometry and Contain a Central Trp Residue as Binding Anchor Point

(A) Photoaffinity labeling experiment using a 22-residue benzophenone-labeled Munc13-1 peptide and purified CaM under reducing conditions. Products of the UV light-induced reaction were analyzed by SDS-PAGE (18%) and Coomassie blue stain. Crosslinking resulted in the appearance of two bands with an apparent molecular mass slightly higher than CaM alone (the nature of these bands was examined by mass spectrometry, see below). Crosslinking was blocked by addition of increasing amounts of unlabeled peptide. (B) Photoaffinity labeling experiment identical to the one described in (A) but using a 22-residue benzophenone-labeled ubMunc13-2 peptide. (C and D) Photo crosslinking reaction products of CaM with Bp-Munc13-1(459–479) (C) and Bp-ubMunc13-2(382–402) (D) were separated by liquid chromatography on a reversed phase column and eluted into the mass spectrometer. The total ion current chromatograms are shown. Brackets indicate the overlapping signals that represent CaM and the photoadducts. Note that a total of three CaM/photoadduct peaks were detected, resembling the data obtained with SDS-PAGE (A and B). The electrospray mass spectra corresponding to the entire CaM/photoadduct signal (in brackets, designated with MS) were transformed to obtain the deconvoluted mass spectra shown in (E) and (F). (E and F) Deconvoluted mass spectra of the photo crosslinking reaction products of CaM with Munc13-1(459–479) (E) and ubMunc13-2(382–402) (F). Only CaM and a 1:1 photoadduct with the respective Munc13 peptide are detected by mass spectrometry. (G) Fluorescence emission scans of 10 μM peptide Munc13-1(459–479). Trp fluorescence was excited at 290 nm. The emission of Munc13-1(459–479) peaked at 355 nm. A blue shift occurred after addition of EGTA/CaM while CaM alone had no significant fluorescence. Addition of excess Ca^{2+} led to a further blueshift and intensity increase, resulting in an emission maximum of 324 nm. (H) Fluorescence emission scans of 10 μM peptide ubMunc13-2 (382–402) as described in (G). A strong blue shift occurred only after addition of Ca^{2+}/CaM but not apoCaM.

Arg-mutated Munc13-GFP fusion proteins in primary hippocampal neurons using Semliki-Forest-Virus expression constructs. Recombinant proteins were immunoprecipitated with a polyclonal anti-GFP antibody and Protein A-Sepharose and tested for Ca^{2+}-dependent binding of CaM and other Munc13 interactors. The mutated proteins were well expressed and intact (Figure 5B), indicating proper folding and stability. Consistent with the results of the GST-cosedimentation experiments, Ca^{2+}-dependent CaM binding was observed with

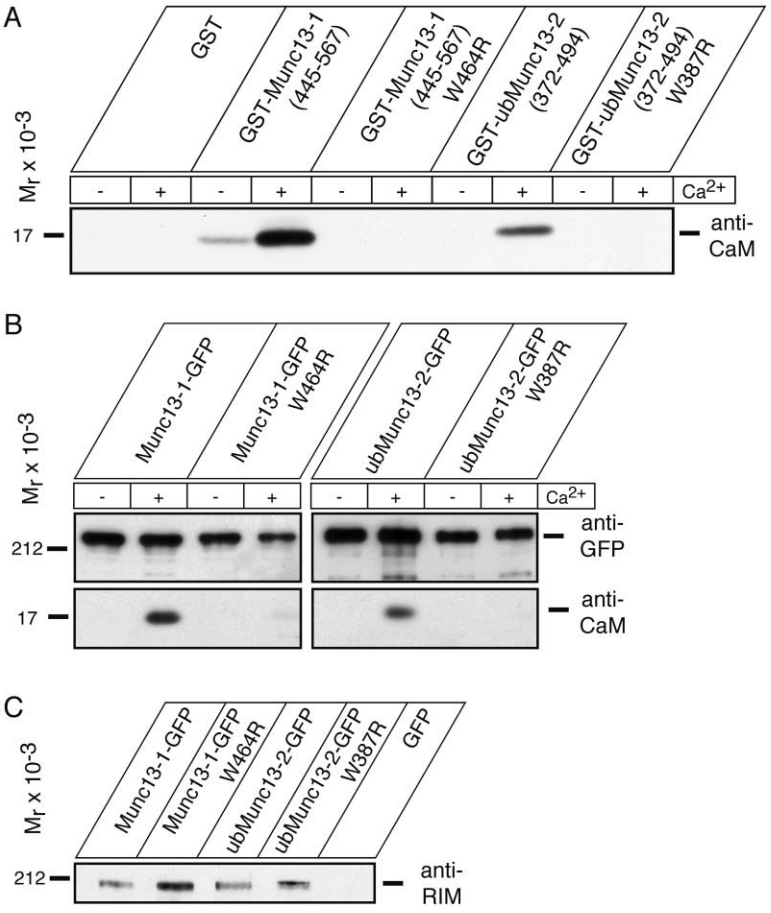

Figure 5. Trp/Arg Mutations within the Amphipathic CaM Binding Helix of Munc13s Abolish CaM Binding

(A) CaM binding to the indicated GST-Munc13 fusion protein was determined in cosedimentation assays as described for Figure 2. CaM binding was robust and specific for wt proteins but not detected for fragments in which the conserved Trp in the amphipathic helix was mutated to Arg.

(B) Immunoblot analysis of immunoprecipitations from cultured primary neurons overexpressing the indicated full-length Munc13-GFP fusion proteins after Semliki-Forest-Virus infection. Immunoprecipitations were performed using a polyclonal anti-GFP antibody. Precipitated material was analyzed by SDS-PAGE and immunoblotting using monoclonal antibodies to CaM and GFP.

(C) Immunoblot analysis of RIM binding in immunoprecipitations as described for (B). RIM binding was similar for wt and CaM-insensitive mutant Munc13 constructs.

wt Munc13 isoforms but not with proteins carrying a Trp/Arg mutation within the CaM binding site (Figure 5B). CaM binding was Ca^{2+} dependent for both full-length Munc13s, while, for the peptide Munc13-1(459–479) and the Munc13-1 fragment GST-Munc13-1(445–567), CaM binding was partially Ca^{2+} independent (compare Figures 2B, 4A, 4G, and 5A, with 5B). This discrepancy may be due to differences in Ca^{2+} sensitivity between peptides and full-length proteins. Alternatively, a weak Ca^{2+}-independent binding may be occluded in cosedimentation and immunoprecipitation experiments.

The binding of RIM to Munc13-1 and ubMunc13-2 was unaffected under all conditions tested (Figure 5C). Thus, the structural integrity of the N termini of Munc13-1 and ubMunc13-2, which contain an extensive N-terminal RIM binding interface (Betz et al., 2001), is not altered by Trp/Arg mutations within the CaM binding site.

Prevention of CaM Binding to Munc13s Affects Short-Term Plasticity

We next studied the function of Ca^{2+}/CaM in modulating Munc13 activity and synaptic strength. Frequency facilitation (i.e., increasing EPSC amplitudes during the high-frequency train) and augmentation (i.e., increased EPSC amplitudes after the high-frequency train) are prominent in hippocampal neurons from Munc13-1 knockout (KO) mice, which express only Munc13-2, and in Munc13-1/2 DKO cells overexpressing ubMunc13-2. These forms of STE associated with ubMunc13-2 expression are sensitive to EGTA (Rosenmund et al., 2002). On the other hand, Munc13-2 KO cells, which express only Munc13-1, and Munc13-1/2 DKO cells overexpressing Munc13-1 show moderate depression (i.e., decreasing EPSC amplitudes) during high-frequency stimulation. These observations indicate a role of Munc13s in determining STP characteristics of synapses.

Considering the numerous neuronal and synaptic CaM targets, pharmacological tools are too unspecific for an investigation of the functional role of the CaM/Munc13 complex. To circumvent this problem, we compared the phenotype of autaptic hippocampal glutamatergic neurons of Munc13-1/2 DKO mice, which are completely release incompetent (Varoqueaux et al., 2002), after rescue with wt or CaM-insensitive Munc13 variants.

Evoked EPSC amplitudes of DKO neurons were rescued by overexpression of wt and CaM-insensitive Munc13 variants (Figure 6A; 2.13 ± 0.22 nA [n = 81] for Munc13-1 versus 2.55 ± 0.26 nA [n = 79] for Munc13-1^{W464R}; 1.56 ± 0.18 nA [n = 54] for ubMunc13-2 versus 2.08 ± 0.23 nA for ubMunc13-2^{W387R} [n = 88]; not significant). The efficient rescue of the EPSC amplitudes upon overexpression of wt and CaM-insensitive Munc13 variants indicates that the Trp/Arg mutation in the amphipathic

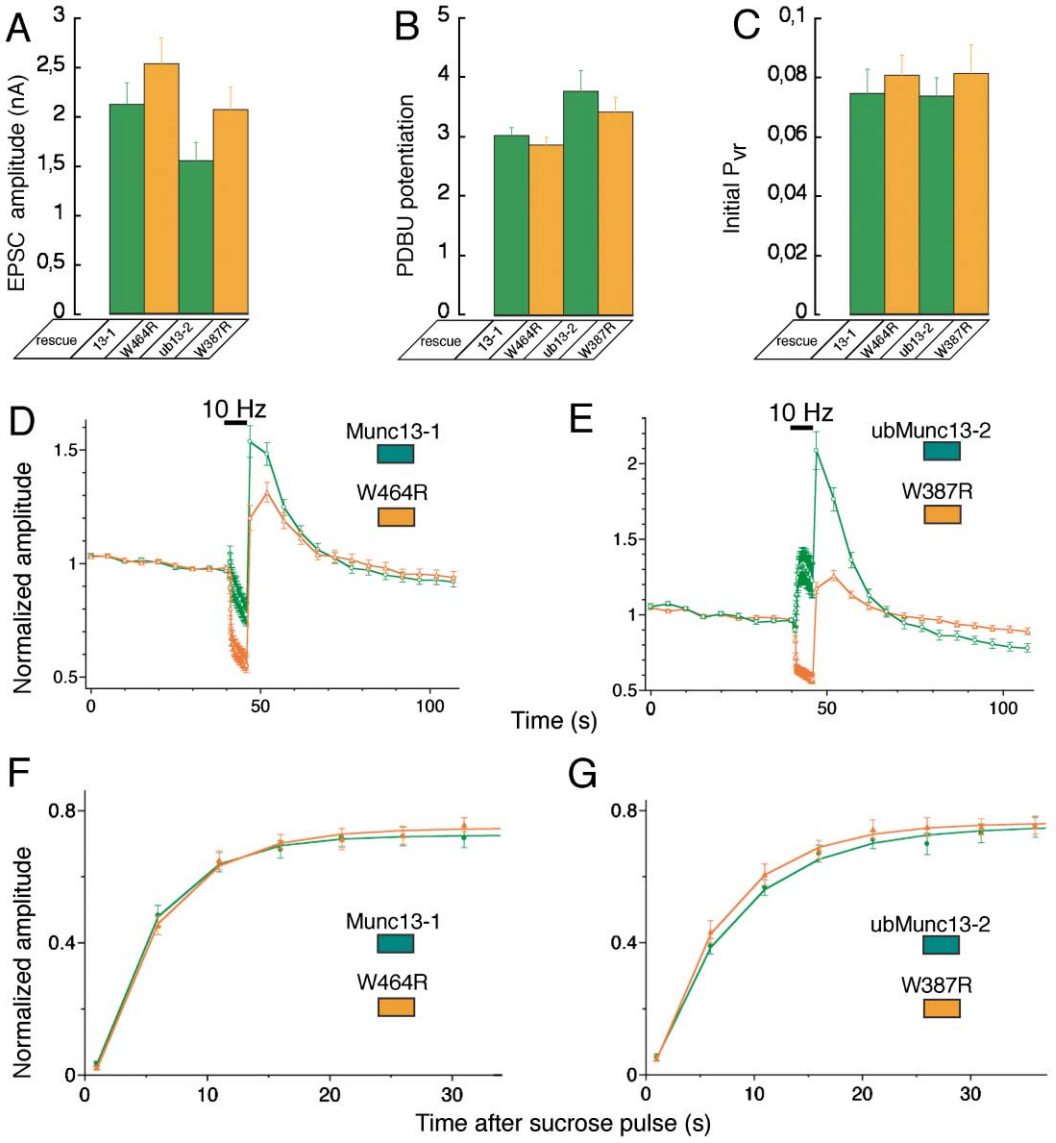

Figure 6. Altered Short-Term Plasticity in Glutamatergic Autaptic Munc13-1/2 DKO Neurons Rescued with Wild-Type or CaM-Insensitive Munc13 Variants

(A) Summary diagram of evoked EPSC amplitudes from hippocampal neurons rescued with the indicated Semliki-Forest-Virus construct. Nonrescued cells were presynaptically completely silent. For each cell, the average EPSC amplitude of 12 pulses at 0.2 Hz was determined. Differences were not significant between wt and mutant groups (n = 54–88).

(B) Summary diagram of the potentiation of evoked EPSC amplitudes after a 70 s application of 1 μM PDBU. Data are normalized to the average EPSC amplitude before PDBU application (n = 21–38). Differences were not significant between wt and mutant groups.

(C) Summary diagram of P_{vr} values of hippocampal neurons rescued with the indicated Semliki-Forest-Virus constructs (n = 19–20). P_{vr} was determined in a sucrose pulse experiment as described in the text. Differences were not significant between wt and mutant groups.

(D) Short-term plasticity of autaptic Munc13-1/2 DKO neurons rescued with wt Munc13-1 or Munc13-1^{W464R}. During a period of basal stimulation at 0.2 Hz, a 10 Hz train was applied for 5 s. The interval between the low- and high-frequency stimulation periods was 2 s. Data are normalized to the average EPSC amplitude of the first nine data points at 0.2 Hz stimulation frequency (n = 78–79). Cells rescued with Munc13-1^{W464R} showed a stronger depression and lack of augmentation.

(E) Short-term plasticity of autaptic Munc13-1/2 DKO neurons rescued with wt ubMunc13-2 or ubMunc13-2^{W387R}. The experiment was performed as described in (D) (n = 54–88). Cells rescued with wt ubMunc13-2 exhibited frequency facilitation and augmentation, while cells rescued with ubMunc13-2^{W387R} showed depression and hardly any augmentation under the same conditions.

(F and G) Recovery of EPSC amplitudes of the indicated cell population during continuous stimulation at 0.2 Hz after a complete depletion of the RRP by a sucrose pulse. Amplitudes are normalized to the average amplitude before application of the sucrose pulse. Data were fitted with a single exponential function (see text). The recovery rates after activity-independent depletion were virtually identical in wt and mutant groups (n = 16–25).

helix of Munc13s does not interfere with expression, protein turnover, synaptic transport, or basal priming function.

We then compared the function of wt and CaM-insensitive Munc13 variants during and after high-frequency stimulation. For that purpose, a 10 Hz train was applied during a period of stimulation at 0.2 Hz. Neurons rescued with wt ubMunc13-2 usually showed frequency facilitation and augmentation, while, in neurons rescued with wt, Munc13-1 depression was prominent (Figures 6D and 6E; Rosenmund et al., 2002). When we compared the CaM-insensitive variants with the respective wt isoforms, we observed striking differences during high-frequency stimulation. Figure 6D shows the normalized EPSC amplitudes of DKO neurons rescued with either Munc13-1 (n = 79) or Munc13-1^{W464R} (n = 78) during and after a 5 s 10 Hz train. Shown are data normalized to the averaged initial amplitudes (nine stimuli evoked at 0.2 Hz) of the indicated cell populations. EPSC amplitudes of neurons overexpressing wt Munc13-1 depressed during the 10 Hz train, finally reaching a level of ~80% of the initial value. Upon return to basal stimulation at 0.2 Hz, which started 2 s after the train, the synaptic amplitudes were initially moderately augmented (1.55-fold of the initial value). However, in neurons rescued with Munc13-1^{W464R}, depression set in instantly during the 10 Hz train and reached a level of ~60% of the initial value, and augmentation following the train was reduced and delayed (1.3-fold as compared to the initial value). The steady-state synaptic amplitudes under conditions of vesicle depletion are determined by the rate of RRP refilling. Thus, the lower steady-state amplitudes as well as the delay in the remaining augmentation of neurons rescued with Munc13-1^{W464R} indicate an impaired priming activity, which, in turn, alters STP (see below).

We investigated the effect of the W387R mutation in ubMunc13-2 under the same conditions as described above. Cells expressing wt ubMunc13-2 exhibited frequency facilitation and augmentation (Figure 6E). On average, amplitudes reached ~130% of the initial value during the 10 Hz train, and the first response following the train was augmented 2.1-fold (n = 54). In contrast, cells expressing ubMunc13-2^{W387R} (n = 88) showed strong depression (~60% of the initial amplitude) and very little or no posttrain augmentation. Thus, CaM insensitivity of Munc13s had dramatic consequences on STP. Differences between the two wt isoforms were eliminated in the CaM-insensitive variants such that STP characteristics were similar for Munc13-1^{W464R} and ubMunc13-2^{W387R}.

An important factor controlling STP characteristics is the vesicular release probability (P_{vr}), which can be determined by the combined measurement of the RRP and evoked EPSCs. The size of the RRP is measured by application of hypertonic sucrose solution, which releases all primed vesicles in a Ca^{2+}-independent manner (Rosenmund and Stevens, 1996). The P_{vr} is the ratio of the charge transfer during an evoked EPSC and the charge transfer during the transient part of the sucrose response. RRP sizes and EPSC charges were similar in both wt and mutant groups (data not shown). Cells expressing wt and CaM-insensitive mutant Munc13s therefore had a similar initial P_{vr} (Figure 6C; 7.5% ± 0.8% [n = 19] for wt Munc13-1 versus 8.1% ± 0.7% [n = 20] for Munc13-1^{W464R}, not significant; 7.4% ± 0.6% [n = 19] for wt ubMunc13-2 versus 8.2% ± 1% ([n = 20] for ubMunc13-2^{W387R}, not significant). Thus, the synaptic depression and strong reduction in augmentation during and after 10 Hz trains in cells expressing CaM-insensitive Munc13 variants are not due to changes in initial P_{vr}.

In the course of the sucrose pulse experiments, we monitored the recovery of EPSC amplitudes during continuous 0.2 Hz stimulation. The recovery kinetics were virtually identical in both wt and mutant groups (Figures 6F and 6G), indicating that CaM-insensitive Munc13 variants mediate normal Ca^{2+}-independent RRP refilling. The recovery kinetics could be fitted with a single exponential function with a time constant of 5–7 s, which is in agreement with previously published data (Rosenmund and Stevens, 1996; Stevens and Wesseling, 1998).

To further verify the specificity of the Trp/Arg mutations, we investigated the functionality of the DAG/PE binding C_1 domains, which are located directly C-terminal of the CaM binding sites in both isoforms. Binding of ligand to the C_1 domain of Munc13s induces a strong potentiation of the EPSC amplitude (Rhee et al., 2002). Thus, PE potentiation of transmitter release can be used to report Munc13 functionality. In hippocampal neurons, a 70 s application of 1 μM PDBU leads to maximal potentiation, which subsequently decays within ~5 min of washout. We found that PE-induced potentiation was similar in neurons rescued with wt and CaM-insensitive Munc13 variants (Figure 6B; 3.03-fold ± 0.14-fold [n = 38] for wt Munc13-1 versus 2.86-fold ± 0.14-fold [n = 26] for Munc13-1^{W464R}, not significant; 3.77-fold ± 0.35-fold [n = 21] for wt ubMunc13-2 versus 3.42-fold ± 0.25-fold [n = 23] for ubMunc13-2^{W387R}, not significant). These data show that the Trp/Arg mutations do not induce nonspecific structural deficits within the flanking C_1 domains of Munc13s.

Together, these experiments indicate that CaM binding to Munc13s is induced during synaptic activity, stimulates Munc13 function, and controls Ca^{2+}-dependent STP. In the absence of all CaM-dependent regulatory processes, the two Munc13 isoforms have similar properties, as their expression then is associated with strong depression during high-frequency activity. Both Munc13 isoforms can be activated such that synapses driven by ubMunc13-2 strongly augment, while synapses driven by Munc13-1 show reduced depression and moderate augmentation during high rates of synaptic activity. Our conclusions are supported by the observation that the CaM antagonist W7 (2 μM) caused a reversible inhibition of facilitation and augmentation in Munc13-1 KO neurons, which only express Munc13-2 (data not shown).

CaM Binding to Munc13s Mediates Ca^{2+}-Dependent Modulation of the RRP Size

We found previously that the different STP phenotypes associated with selective expression of either Munc13-1 or ubMunc13-2 are not caused by differences in the initial P_{vr} (Rosenmund et al., 2002). Here, we show that the strong depression and lack of augmentation associated with CaM-insensitive Munc13s are also not due to altered initial P_{vr} (Figure 6C). Our previous analysis of Munc13-1 KO neurons revealed that two factors contribute equivalently to the augmentation after a 10 Hz train,

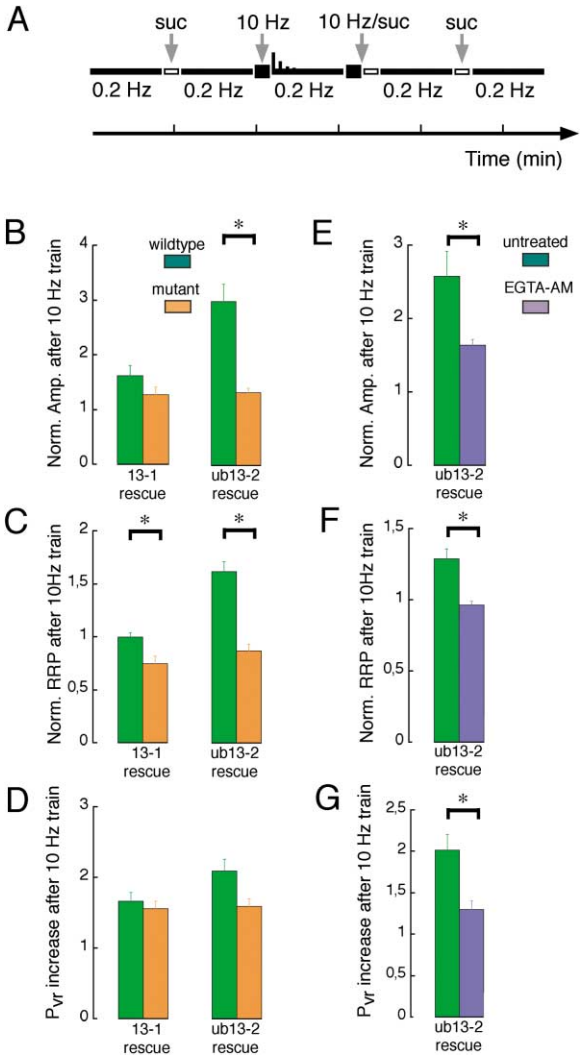

Figure 7. Impaired Ca^{2+}-Dependent RRP Size Modulation in Neurons Rescued with CaM-Insensitive Munc13 Variants

(A) View of the experimental design used to determine P_{vr} and the RRP under conditions of augmentation. The RRP and augmented EPSC were measured 2 s after a 10 Hz train with 50 stimuli and normalized to the averaged RRP under basal conditions. The basal RRP was determined once before and once after the experiments to correct for the rundown associated with repeated sucrose application.

(B) Augmentation of EPSC amplitudes 2 s after the 10 Hz train. Cells rescued with wt Munc13-1 showed moderate augmentation, and cells rescued with wt ubMunc13-2 showed strong augmentation. Augmentation was strongly reduced in both CaM-insensitive mutants (n = 11–16; asterisk indicates significance).

(C) Changes in the RRP size under conditions of augmentation. Values are normalized to the RRP size under basal conditions. When expressing CaM-insensitive Munc13 variants, we observed incomplete refilling of the RRP within 2 s after the 10 Hz train, while expression of the CaM-sensitive wt variants led on average to full refilling or even RRP size expansion in individual cells (n = 12–16).

(D) Changes in the P_{vr} under conditions of augmentation. Values are normalized to the initial P_{vr} under basal conditions. The P_{vr} was increased subsequent to the 10 Hz train irrespective of the CaM sensitivity or Munc13 isoform (n = 12–14). Differences between wt and mutant groups were not significant.

(E) Augmentation of EPSC amplitudes 2 s after a 10 Hz train with 25 stimuli in cells rescued with ubMunc13-2. One group of cells was preincubated in 100 μM EGTA-AM for 20 min at RT. The augmentation was significantly reduced by the membrane-permeable Ca^{2+} chelator (n = 8–10).

(F) Changes in the RRP size under conditions of augmentation normalized to the RRP under basal conditions and effect of EGTA-AM on this parameter. The RRP expansion observed in ubMunc13-2-expressing cells was significantly reduced after EGTA-AM treatment (n = 8–10).

(G) Changes in the P_{vr} under conditions of augmentation normalized to the P_{vr} under basal conditions and effect of EGTA-AM on this parameter. The increase in P_{vr} after the 10 Hz train was significantly reduced after EGTA-AM treatment (n = 8–10).

i.e., an increase in the RRP and an increase in P_{vr} during and after high-frequency stimulation (Rosenmund et al., 2002). We therefore tested whether changes in the activity-dependent modulation of one of these parameters are associated with the phenotype of cells expressing CaM-insensitive Munc13 mutants.

To separately analyze activity-dependent changes of the RRP and P_{vr}, we determined the RRP size and P_{vr} 2 s after a 10 Hz train with 50 stimuli. Because of the slight rundown of EPSCs associated with sucrose application, the pool size under basal conditions was determined twice, once at the beginning and once at the end of the experiment, and averaged. Between these two sucrose applications, the augmented EPSC amplitude (after a first 10 Hz train) and the augmented RRP (after a second 10 Hz train) were determined (Figure 7A). The augmented RRP size was normalized to the averaged RRP size under basal conditions and provides, together with the augmented EPSC charge, an estimate of the P_{vr} under conditions of augmentation (P_{vr} = EPSC charge/sucrose charge).

Posttrain augmentation of evoked EPSC amplitudes in rescued cells was 1.64-fold ± 0.19-fold (n = 13) for wt Munc13-1 versus 1.28-fold ± 0.14-fold (n = 11) for Munc13-1^{W464R} (not significant) (Figure 7B) and 3.1-fold ± 0.33-fold (n = 14) for wt ubMunc13-2 versus 1.38-fold ± 0.08-fold (n = 16) for ubMunc13-2^{W387R} ($p < 0.001$) (Figure 7B).

The analysis of the RRP size modulation during augmentation showed dramatic differences between neurons rescued with CaM-sensitive and CaM-insensitive Munc13s. The RRP size under conditions of augmentation varied from 1.3- to 0.73-fold in cells expressing wt Munc13-1 and was, on average, unchanged (1.01-fold ± 0.04-fold, n = 13, normalized to the basal RRP size) (Figure 7C). The RRP size upon Munc13-1^{W464R} expression was significantly reduced 2 s after the 10 Hz train, indicating incomplete recovery after the partial depletion. The average RRP size reduction under conditions of augmentation was 0.75-fold ± 0.07-fold (n = 12, $p < 0.001$), and none of the cells within this group showed an RRP size increase (Figure 7C). RRP size modulation was even more prominent in cells expressing ubMunc13-2 variants. Here, an average RRP size increase was detected upon ubMunc13-2 overexpression (1.62-fold ± 0.09-fold, n = 15) versus a 0.87-fold ± 0.07-fold decrease (n = 16) with ubMunc13-2^{W387R} expression ($p < 0.001$) (Figure 7C). Together with the fact that basal refilling rates are not affected by CaM insensitivity of Munc13s (Figures 6F and 6G), these data show that accelerated RRP refilling mechanisms and accom-

panying increases in RRP size are impaired by prevention of CaM/Munc13 binding. The lack of activity-dependent modulation of RRP sizes indicates that Ca^{2+}/CaM activates the priming activity of Munc13s, which has extensive consequences on STP.

Analysis of the vesicular release probability P_{vr} revealed that P_{vr} in the augmented state was increased similarly in cells expressing Munc13-1 (1.68-fold ± 0.12-fold, n = 13) and Munc13-1^{W464R} (1.56-fold ± 0.11-fold [n = 12], not significant) (Figure 7D). Likewise, cells expressing CaM-sensitive and CaM-insensitive variants exhibited similar increases of P_{vr} in the augmented state (2.1-fold ± 0.17-fold [n = 14] for ubMunc13-2 versus 1.64-fold ± 0.1-fold [n = 16] for ubMunc13-2^{W387R}, not significant) (Figure 7D). These data show that increases in P_{vr} during and after high-frequency trains are independent of the CaM sensitivity of Munc13s.

While activity- and Ca^{2+}-dependent acceleration of RRP refilling rates has been reported earlier (Dittman and Regehr, 1998; Stevens and Wesseling, 1998; Wang and Kaczmarek, 1998), a role for CaM in this process has only recently been suggested (Sakaba and Neher, 2001). Our finding that neurons rescued with CaM-insensitive Munc13 variants exhibit a lack of activity-mediated increases in vesicle priming indicates that a CaM/Munc13 complex is the transducer that mediates Ca^{2+} signaling to the vesicle-priming machinery. A prediction of this interpretation is that intracellular Ca^{2+} chelators mimic the effect of CaM insensitivity of the Munc13-dependent vesicle-priming machinery. We preincubated cells rescued with ubMunc13-2 for 20 min at room temperature with 100 μM EGTA-AM. To avoid depletion of the Ca^{2+} buffer during the experiment described in Figure 7A, we only applied 25 stimuli at 10 Hz. Augmentation of untreated cells was 2.58-fold ± 0.34-fold (n = 8) versus 1.64-fold ± 0.076-fold (n = 10) in the EGTA-AM group (Figure 7E). Thus, intracellular Ca^{2+} was effectively buffered and augmentation reduced significantly ($p < 0.05$). We next determined the effect of this pharmacological manipulation on P_{vr} and RRP size under conditions of augmentation. Normalized augmented pool sizes were 1.29 ± 0.07 (n = 8) in untreated cells versus 0.96 ± 0.03 (n = 10) in EGTA-AM-treated cells ($p < 0.001$) (Figure 7F). Normalized P_{vr} under conditions of augmentation was 2.01 ± 0.19 (n = 8) versus 1.3 ± 0.1 in EGTA-AM-treated cells ($p < 0.01$) (Figure 7G). The initial P_{vr} was also reduced in the EGTA-AM-treated group (3.0% ± 0.8% [n = 10] versus 9.2% ± 1.7% [n = 8] in untreated cells [$p < 0.01$]). Thus, increased Ca^{2+} buffering not only mimics the effects of CaM insensitivity of Munc13s but also alters the initial P_{vr} by reducing the free intracellular Ca^{2+} concentration.

Discussion

Our YTH (Figure 1) and biochemical data (Figures 2, 4, and 5) demonstrate that Munc13-1 and ubMunc13-2 bind CaM in a Ca^{2+}-dependent manner. The amphipathic helix that serves as the CaM binding site in the two Munc13s is evolutionarily conserved, and its structure and functional characteristics with a central essential Trp residue resemble those of CaM binding sites in other CaM targets (Figure 3). CaM is colocalized with Munc13s in the presynaptic compartment. It is inactive at resting [Ca^{2+}] of about 100 nM in eukaryotic cells but is rapidly activated in domains of elevated [Ca^{2+}] in the range of ~500 nM (Chin and Means, 2000). In view of these characteristics and the fact that Ca^{2+} levels are exquisitely regulated in presynaptic compartments within a concentration range to which CaM is sensitive, Munc13s are likely important physiological signaling targets of CaM in the presynapse.

We examined the function of the CaM/Munc13 complex by rescue of Munc13-1/2 DKO cells that overexpressed wt Munc13s or CaM-insensitive Munc13 variants. CaM-insensitive Munc13 variants were obtained by mutation of a characteristic Trp residue in the CaM binding motif of both isoforms. An important anchoring role for this residue in CaM/Munc13 recognition was inferred from its altered fluorescence emission upon CaM binding (Figures 4G and 4H) and from the structure of CaM targets with similar motifs (Chin and Means, 2000). We mutated the corresponding Trp residues in Munc13s to helix-promoting Arg residues to block CaM binding but stabilize the α-helical organization of the CaM binding site. Indeed, CaM binding in Munc13 variants with a Trp/Arg mutation in the CaM binding site was blocked (Figure 5A), but no additional, nonspecific effects on the integrity or function of the protein were found (Figures 5B, 5C, 6A, and 6B). The molecular characterization of the CaM binding sites in Munc13s by mutagenesis allowed us to design a genetic approach to analyze the functional role of CaM binding, independently of the nonspecific pharmacological tools available for interference with CaM function.

The present (Figures 6D and 6E) and a previous study (Rosenmund et al., 2002) show that the specific equipment of synapses with different Munc13s determines STP characteristics. We used autaptic hippocampal neurons as a genetically accessible model system to investigate the role of Munc13s in synaptic depression, frequency facilitation, and augmentation, forms of STP that are expressed in this preparation. In contrast to paired-pulse facilitation, which develops instantaneously, is dependent on the initial release probability, and is likely to be caused by passive influences on Ca^{2+} dynamics (Felmy et al., 2003), Munc13-associated frequency facilitation and augmentation are independent of the initial release probability (Augustin et al., 1999) (Figure 6B). The onset of ubMunc13-2-associated frequency facilitation is in the range of 100 ms, and augmentation decays with a time constant of ~8 s (Rosenmund et al., 2002). A similar but weaker form of enhancement is associated with Munc13-1-driven synapses, indicating that both Munc13s are subject to a similar activation during sustained activity. Here we show that this activation of Munc13s is mediated by CaM binding and leads to attenuation of depression in the case of Munc13-1 and to frequency facilitation and augmentation in the case of ubMunc13-2 (Figures 6D and 6E).

Our analysis of the dynamic changes of the RRP size and of the P_{vr} under conditions of augmentation indicate that both parameters are modified during sustained synaptic activity in wt-like synapses. Only one of both mechanisms, the activity-dependent modulation of the RRP, is impaired in cells rescued with CaM-insensitive

Munc13 variants, while increases of P_{vr} remain unaffected by disruption of the CaM/Munc13 complex (Figures 7C and 7D). The observations that the RRP of cells rescued with CaM-insensitive Munc13 variants is not fully recovered within 2 s after a partial depletion by sustained activity and that these cells recover with normal rates from activity-independent depletion (Figures 6F and 6G) indicate that activity-dependent RRP refilling is specifically impaired by CaM insensitivity. As expected for a CaM-mediated mechanism, this effect can be mimicked by increased intracellular Ca^{2+} buffering, demonstrating that the activity-dependent refilling is indeed Ca^{2+} dependent. The finding that the size of the RRP can be increased in response to activity (more than double in individual cells) is in line with an equilibrium model of priming in which the size of the RRP is determined by the priming and unpriming rates. According to such a model, an acceleration of the priming rate would result in a shift in the equilibrium and cause an increased RRP size.

Our experiments separate two mechanisms that shape STP characteristics of synapses. One is defined by the action of the newly identified CaM/Munc13 complex, which mediates activity-dependent vesicle priming and modulation of the RRP size. The CaM/Munc13 complex is likely the molecular correlate of the Ca^{2+}-dependent refilling mechanism that has been observed in several vertebrate preparations (Dittman and Regehr, 1998; Stevens and Wesseling, 1998; Wang and Kaczmarek, 1998) and in an invertebrate preparation (Kusano and Landau, 1975). A second Ca^{2+}-dependent mechanism controls modulation of P_{vr} during sustained synaptic activity and likely involves the low-affinity secretory Ca^{2+} sensor. Both Ca^{2+}-dependent mechanisms are sensitive to modulation of the residual Ca^{2+} signal, e.g., by increased Ca^{2+} buffering (Figures 7F and 7G).

Although Ca^{2+}-dependent acceleration of RRP refilling has been described, its role in STP is poorly understood. The present study indicates that impaired RRP refilling during sustained activity has dramatic consequences on STP, i.e., more pronounced depression in Munc13-1-driven synapses and a switch from frequency facilitation to depression in ubMunc13-2-driven synapses (Figures 6D and 6E). Thus, acceleration of the RRP refilling rate by Munc13s is not a cause for one specific STP phenomenon. Instead, the rate of Munc13-mediated RRP refilling could shape all those forms of STP that are neither too fast (i.e., expressed before RRP refilling can occur) nor too long lasting (i.e., maintained after the Ca^{2+}-dependent activation of the refilling mechanism has relaxed). Our results are consistent with a mathematical model of synapses that takes into account a Ca^{2+}-dependent increase of P_r and a Ca^{2+}-dependent acceleration of RRP refilling. Such a model describes the behavior of a number of synapses in different preparations (Dittman et al., 2000).

Formally, we can link the function of the CaM/Munc13 complex only to the Ca^{2+}-dependent modulation of the RRP size in our autaptic neuron model system. However, two lines of evidence indicate that the function of this complex may be similar in other types of synapses. First, UNC-13/Munc13s are conserved and widely expressed key synaptic proteins whose function in synaptic vesicle priming has been verified in mouse, worm, and fly synapses. CaM, on the other hand, is ubiquitously expressed in eukaryotic cells and coexpressed with UNC-13/Munc13s. The finding that the CaM recognition motif is conserved in invertebrate and vertebrate members of the gene family indicates a conserved function of this structural element (Figure 3C; Xu et al., 1998). UNC13/Munc13 proteins likely regulate the conformation of Syntaxin and thus the assembly of the synaptic SNARE complex, another presynaptic element that is remarkably conserved during evolution. Activation of Munc13 function by CaM may increase the ability of Munc13s to control SNARE complex formation. Thus, all elements of the Ca^{2+}-dependent refilling mechanism proposed here, including the Ca^{2+} sensor/effector complex and the downstream targets in the release machinery, are evolutionarily conserved. Second, Ca^{2+}-dependent refilling of the RRP was examined in a variety of vertebrate and invertebrate synapses. The fact that accelerated RRP refilling is sensitive to CaM inhibitors in the Calyx of Held (Sakaba and Neher, 2001) indicates that, at least in some of these synapses, the same CaM/Munc13-dependent molecular mechanism is operating.

In summary, the present study identifies an evolutionarily conserved molecular correlate for a Ca^{2+}-dependent RRP refilling mechanism that determines presynaptic output during sustained activity and shapes different types of STP, including depression and forms of enhancement.

Experimental Procedures

YTH Screens

YTH bait vectors were constructed in pLexN. Corresponding vectors encode Munc13 fragments as N-terminal fusion proteins with the LexA DNA binding domain. YTH control experiments and YTH screens using pLexN baits, rat brain cDNA libraries in pVP16-3 (encoding fusion proteins with an N-terminal VP16 transcriptional activation domain), and the L40 yeast strain were performed as described (Betz et al., 1997).

Expression Vectors

Bacterial expression vectors encoding GST in frame with Munc13 fragments were constructed in pGexKG. Bacterial expression and purification of fusion proteins were performed according to published procedures (Betz et al., 2001). Mutations in the CaM binding site and C_1 domain of Munc13s were introduced using QuikChange (Stratagene). Semliki-Forest-Virus expression vectors encoding Munc13 variants in frame with a C-terminal EGFP tag were constructed in pSFV1 (GIBCO-BRL).

Cosedimentation Assays and Immunoprecipitations

For GST cosedimentation experiments, crude synaptosomes from rat brain were solubilized at a protein concentration of 2 mg/ml in 50 mM Tris (pH 8), 150 mM NaCl, 1 mM EGTA, 1% Igepal (Sigma), 0.2 mM PMSF, 1 μg/ml aprotinin, and 0.5 μg/ml leupeptin. After stirring on ice, insoluble material was removed by centrifugation (60 min at 250,000 × g_{max}). The equivalent of 4 mg total extracted protein was then incubated with 20 μg of immobilized GST-Munc13 fusion protein in the presence or absence of 2 mM free Ca^{2+} for 2 hr at 4°C. Beads were then washed three times with solubilization buffer containing 0.1% Igepal in the presence or absence of Ca^{2+}, resuspended in 100 μl SDS-PAGE sample buffer, and analyzed by SDS-PAGE and immunoblotting. Immunoblots for CaM were performed according to a protocol from Sigma using an anti-CaM antibody from Upstate Biotechnologies. For coimmunoprecipitation assays, Munc13-EGFP fusion constructs were expressed for 18 hr after Semliki-Forest-Virus infection in mouse hippocampal neurons grown on a confluent glia cell layer (8 DIV) (see below). Cells were solubilized as described above, including a protease inhibitor mix

(Calbiochem), and centrifuged at 4°C for 15 min at 15,000 rpm on a tabletop centrifuge to remove insoluble material. Aliquots of extracts were then mixed with 5 μl polyclonal anti-GFP antibody (Clontech) and 20 μl Protein A-Sepharose and incubated for 1 hr at 4°C in the presence or absence of 2 mM free Ca^{2+}. Beads were washed as described above, resuspended in 60 μl SDS PAGE sample buffer, and analyzed by SDS PAGE and immunoblotting.

Peptide Synthesis, Photoaffinity Labeling, Mass Spectrometry, and Fluorescence Spectrophotometry

Peptides (N-terminally elongated by an artificial Cys residue) were synthesized and characterized using standard procedures (Jahn et al., 2001). The benzophenone photophore was introduced by N-terminal modification using parabenzoylbenzoic acid N-hydroxysuccinimide ester (Jahn et al., 2002). Peptide stocks were prepared in 10 mM aqueous acetic acid, and final peptide concentrations were determined by amino acid analysis. For photoaffinity labeling, bovine brain CaM (5 μM; Sigma) and the peptidic photoprobe (4.5 μM) were incubated for 2 hr under light exclusion in 250 mM ammonium acetate (pH 8), 5 mM DTT. Reactions were performed in the presence of 3 mM free Ca^{2+} or 2 mM EGTA. The photophore was activated with UV light as described (Jahn et al., 2002). After irradiation, the photoreaction mixtures were analyzed by SDS-PAGE and LC-MS. Before injection into the LC-MS system, protein samples were desalted (RP C18 ZipTips, Millipore). LC-MS of protein mixtures was carried out on a Vydac C4 column (0.3 × 150 mm) as described (Jahn et al., 2001). Eluents were infused into the elctrospray interface of an AutoSpec-T four-sector tandem mass spectrometer (Micromass Waters). The Maximum Entropy algorithm included in the instrument's data system was used to deconvolute the mass spectra. Fluorescence emission scans were measured on an Aminco Bowman Series 2 spectrometer. Excitation was set at 290 ± 3 nm, and emission light was collected at 300–430 ± 3 nm. Peptides were dissolved at 10 μM in 250 mM ammonium acetate (pH 8), 1 mM EGTA. Scans were corrected for background fluorescence and the nonlinearity of the photomultiplier response.

Neuron Cultures and Electrophysiology

Munc13-1 and Munc13-2 knockout mice were published previously (Augustin et al., 1999; Varoqueaux et al., 2002). Microisland cultures of mouse hippocampal neurons were prepared and cultured as described (Pyott and Rosenmund, 2002). This procedure is an optimization of the technique that was used in a previous study (Rosenmund et al., 2002). Semliki-Forest-Virus infections were performed as published (Rosenmund et al., 2002). Sucrose pulse experiments and PE stimulation experiments were performed as described (Rhee et al., 2002; Rosenmund et al., 2002). EGTA-AM (Calbiochem) was used for 20 min preincubation (RT) of cells at a concentration of 100 μM in external solution. Infected cells were measured 18–26 hr postinfection. Data acquisition and analysis were performed as described (Pyott and Rosenmund, 2002). Data are expressed as mean ± SEM. Because of differences in the standard deviation of the EPSC amplitude distributions between both wt and mutant groups, we tested significance with a nonparametric unpaired Mann-Whitney test. P values < 0.05 were considered significant.

Acknowledgments

We thank S. Handt, I. Herfort, I. Thanhäuser, L. van Werven, and T. Liepold for excellent technical assistance. We are grateful to R. Schneggenburger and J. Putkey for valuable discussions. This work was supported by the German Research Foundation (SFB406/A1 to N.B.) and by the Max-Planck-Society.

Received: November 3, 2003
Revised: June 17, 2004
Accepted: June 17, 2004
Published: August 5, 2004

References

Abbott, L.F., Varela, J.A., Sen, K., and Nelson, S.B. (1997). Synaptic depression and cortical gain control. Science *275*, 220–224.

Aravamudan, B., Fergestad, T., Davis, W.S., Rodesch, C.K., and Broadie, K. (1999). Drosophila UNC-13 is essential for synaptic transmission. Nat. Neurosci. *2*, 965–971.

Augustin, I., Rosenmund, C., Sudhof, T.C., and Brose, N. (1999). Munc13-1 is essential for fusion competence of glutamatergic synaptic vesicles. Nature *400*, 457–461.

Betz, A., Okamoto, M., Benseler, F., and Brose, N. (1997). Direct interaction of the rat unc-13 homologue Munc13-1 with the N terminus of syntaxin. J. Biol. Chem. *272*, 2520–2526.

Betz, A., Thakur, P., Junge, H.J., Ashery, U., Rhee, J.S., Scheuss, V., Rosenmund, C., Rettig, J., and Brose, N. (2001). Functional interaction of the active zone proteins Munc13-1 and RIM1 in synaptic vesicle priming. Neuron *30*, 183–196.

Brose, N., Rosenmund, C., and Rettig, J. (2000). Regulation of transmitter release by Unc-13 and its homologues. Curr. Opin. Neurobiol. *10*, 303–311.

Chin, D., and Means, A.R. (2000). Calmodulin: a prototypical calcium sensor. Trends Cell Biol. *10*, 322–328.

Chung, S., Li, X., and Nelson, S.B. (2002). Short-term depression at thalamocortical synapses contributes to rapid adaptation of cortical sensory responses in vivo. Neuron *34*, 437–446.

Cook, D.L., Schwindt, P.C., Grande, L.A., and Spain, W.J. (2003). Synaptic depression in the localization of sound. Nature *421*, 66–70.

Dittman, J.S., and Regehr, W.G. (1998). Calcium dependence and recovery kinetics of presynaptic depression at the climbing fiber to Purkinje cell synapse. J. Neurosci. *18*, 6147–6162.

Dittman, J.S., Kreitzer, A.C., and Regehr, W.G. (2000). Interplay between facilitation, depression, and residual calcium at three presynaptic terminals. J. Neurosci. *20*, 1374–1385.

Eccles, J.C., Katz, B., and Kuffer, S.W. (1941). Nature of the 'endplate potential' in curarized muscle. J. Neurophysiol. *4*, 362–387.

Felmy, F., Neher, E., and Schneggenburger, R. (2003). Probing the intracellular calcium sensitivity of transmitter release during synaptic facilitation. Neuron *37*, 801–811.

Feng, T.P. (1941). The changes in the end-plate potential during and after prolonged stimulation. Chin. J. Physiol. *13*, 79–107.

Jahn, O., Eckart, K., Sydow, S., Hofmann, B.A., and Spiess, J. (2001). Pharmacological characterization of recombinant rat corticotropin releasing factor binding protein using different sauvagine analogs. Peptides *22*, 47–56.

Jahn, O., Eckart, K., Brauns, O., Tezval, H., and Spiess, J. (2002). The binding protein of corticotropin-releasing factor: ligand-binding site and subunit structure. Proc. Natl. Acad. Sci. USA *99*, 12055–12060.

Katz, B., and Miledi, R. (1968). The role of calcium in neuromuscular facilitation. J. Physiol. *195*, 481–492.

Koushika, S.P., Richmond, J.E., Hadwiger, G., Weimer, R.M., Jorgensen, E.M., and Nonet, M.L. (2001). A post-docking role for active zone protein Rim. Nat. Neurosci. *4*, 997–1005.

Kusano, K., and Landau, E.M. (1975). Depression and recovery of transmission at the squid giant synapse. J. Physiol. *245*, 13–22.

Liley, A.W., and North, K.A. (1953). An electrical investigation of repetitive stimulation on mammalian neuromuscular junction. J. Neurophysiol. *16*, 509–527.

Nadim, F., and Manor, Y. (2000). The role of short-term synaptic dynamics in motor control. Curr. Opin. Neurobiol. *10*, 683–690.

O'Neil, K.T., and DeGrado, W.F. (1989). The interaction of calmodulin with fluorescent and photoreactive model peptides: evidence for a short interdomain separation. Proteins *6*, 284–293.

Pyott, S.J., and Rosenmund, C. (2002). The effects of temperature on vesicular supply and release in autaptic cultures of rat and mouse hippocampal neurons. J. Physiol. *539*, 523–535.

Rhee, J.S., Betz, A., Pyott, S., Reim, K., Varoqueaux, F., Augustin, I., Hesse, D., Sudhof, T.C., Takahashi, M., Rosenmund, C., and Brose, N. (2002). Beta phorbol ester- and diacylglycerol-induced augmentation of transmitter release is mediated by Munc13s and not by PKCs. Cell *108*, 121–133.

Rhoads, A.R., and Friedberg, F. (1997). Sequence motifs for calmodulin recognition. FASEB J. *11*, 331–340.

Richmond, J.E., Davis, W.S., and Jorgensen, E.M. (1999). UNC-13 is required for synaptic vesicle fusion in C. elegans. Nat. Neurosci. *2*, 959–964.

Richmond, J.E., Weimer, R.M., and Jorgensen, E.M. (2001). An open form of syntaxin bypasses the requirement for UNC-13 in vesicle priming. Nature *412*, 338–341.

Rosenmund, C., and Stevens, C.F. (1996). Definition of the readily releasable pool of vesicles at hippocampal synapses. Neuron *16*, 1197–1207.

Rosenmund, C., Sigler, A., Augustin, I., Reim, K., Brose, N., and Rhee, J.S. (2002). Differential control of vesicle priming and short-term plasticity by Munc13 isoforms. Neuron *33*, 411–424.

Sakaba, T., and Neher, E. (2001). Calmodulin mediates rapid recruitment of fast-releasing synaptic vesicles at a calyx-type synapse. Neuron *32*, 1119–1131.

Stevens, C.F., and Wesseling, J.F. (1998). Activity-dependent modulation of the rate at which synaptic vesicles become available to undergo exocytosis. Neuron *21*, 415–424.

Varoqueaux, F., Sigler, A., Rhee, J.S., Brose, N., Enk, C., Reim, K., and Rosenmund, C. (2002). Total arrest of spontaneous and evoked synaptic transmission but normal synaptogenesis in the absence of Munc13-mediated vesicle priming. Proc. Natl. Acad. Sci. USA *99*, 9037–9042.

Wang, L.Y., and Kaczmarek, L.K. (1998). High-frequency firing helps replenish the readily releasable pool of synaptic vesicles. Nature *394*, 384–388.

Xu, X.Z., Wes, P.D., Chen, H., Li, H.S., Yu, M., Morgan, S., Liu, Y., and Montell, C. (1998). Retinal targets for calmodulin include proteins implicated in synaptic transmission. J. Biol. Chem. *273*, 31297–31307.

Zucker, R.S., and Regehr, W.G. (2002). Short-term synaptic plasticity. Annu. Rev. Physiol. *64*, 355–405.